

Original article

The effect of supercritical CO₂ on failure mechanisms of hot dry rock

Honglian Li^{1,2,3}, Xiang Jiang⁴*, Zijie Xu^{1,2}, Stephen Bowden³*

¹State Key Laboratory of Coal Mine Disaster Dynamics and Control, Chongqing University, Chongqing 400044, P. R. China

²School of Resources and Safety Engineering, Chongqing University, Chongqing 400044, P. R. China

³School of Geosciences, University of Aberdeen, Scotland, AB24 3UE, United Kingdom

⁴School of Materials Science and Engineering, Chongqing Jiaotong University, Chongqing 400074, P. R. China

Keywords:

Hot dry rock
supercritical CO₂
failure mechanism
statistical distributions
power law

Cited as:

Li, H., Jiang, X., Xu, Z., Bowden, S. The effect of supercritical CO₂ on failure mechanisms of hot dry rock. *Advances in Geo-Energy Research*, 2022, 6(4): 324-333.

<https://doi.org/10.46690/ager.2022.04.07>

Abstract:

Hot dry rock is a clean, renewable resource of geothermal energy with good stability and a high utilization rate. Supercritical CO₂ has shown promising results for improving the permeability and heat exchange of hot dry rock. In order to demonstrate the effect of supercritical CO₂ on the failure mechanism of granite, the acoustic emission of granite during its failure process were studied in addition to X-ray diffraction, scanning electron microscopy, and optical electron microscopy investigations. The experimental results showed that for granite without supercritical CO₂ treatment, as it approached failure, there were many acoustic emission events with a waiting time less than 0.0001 s, and that the power law exponent of the acoustic emission energy distribution decreased. The failure mechanisms were a combination of fracture and friction, with fracturing dominant. After immersion in supercritical CO₂, new cracks and pores appeared in the granite due to the dissolution of minerals, but friction was also a factor evidenced in particle crumbling. Generally, the acoustic emission statistical distributions of granite before and after supercritical CO₂ soaking conformed to the seismic statistical distribution law. This study is conducive to increasing the understanding of artificial earthquakes induced by the development of hot dry rock.

1. Introduction

Hot dry rock is a stable clean renewable energy resource with high utilization efficiency (Beckers et al., 2014; Hofmann et al., 2014). It occurs underground at depths of 3-8 km, and is metamorphic or crystalline rock masses such as granite. Reserves of hot dry rock can provide thermal energy equivalent to 30 times that of all global oil, gas, and coal reserves (Xu et al., 2012). Presently, enhanced geothermal systems are widely used to exploit hot dry rock; that is, hydraulic fracturing is used to improve the permeability and heat exchange area of the fracture system (Duchane and Brown, 2002; Legarth et al., 2005; Garcia et al., 2016).

However, the use of this technology requires a considerable volume of water. For example, 20,000 m³ of water

is required for single well fracturing in GeneSye (Germany) (Hou et al., 2012), 20,000-40,000 m³ of water was required to fracture a single well in Soultz, France (Baisch et al., 2006), and 50,000 m³ of water was required for a single well in Basel, Switzerland (Haering et al., 2008). In addition, there is also a risk of inducing earthquakes during the process of hydraulic fracturing (Anyim and Gan, 2020). A series of such earthquakes have been induced in many places, such as the United Kingdom, France, and South Korea (British Columbia Oil and Gas Commission, 2012; Kim et al., 2018). With the development of mining technology and owing to its excellent physical and chemical properties, supercritical CO₂ has gradually received interest and has become a popular research topic in hot dry fracturing media (Luo et al., 2014; Bongole et al., 2019).

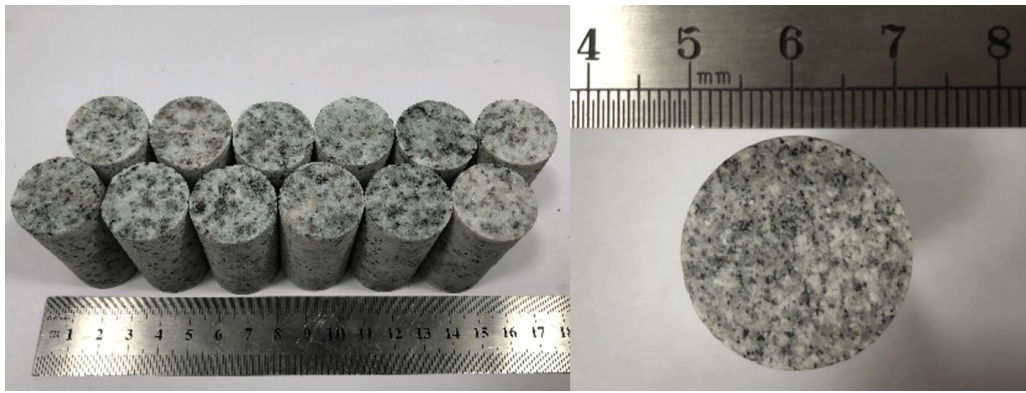


Fig. 1. Granite specimens.

Many studies have shown that when shale, sandstone, and granite are exposed to supercritical CO₂, the compressive strength and elastic modulus of the rocks decrease (Yin et al., 2017; Ershadnia et al., 2020; Li et al., 2020b). The influence of supercritical CO₂ on the failure mechanism of hot dry rock is the premise of understanding earthquakes caused by the supercritical CO₂ fracturing of hot dry rock. Rock particle cracks and seismic plates have similar fractal structures, and their statistical physical responses have consistent avalanche dynamic characteristics (Sathar et al., 2012; Baró et al., 2013). This indicates that statistical physical analysis methods could be used to predict large-scale engineering phenomena through research results in a laboratory. As a sensitive nondestructive detection technology, acoustic emission (AE) technology can capture the energy released by rocks in the process of deformation and failure, hence reflecting the failure mechanism of the rock (Eberhardt et al., 1999; Kim et al., 2015; Zhang et al., 2015). Under stress conditions, the expansion of microcracks and the dislocation of mineral particles in the rock can generate a large number of AE singles. Further penetration of microcracks can lead to sudden failure of the rock, which can be regarded as an “earthquake” at different scales. The AE energy sequence is similar to the earthquake magnitude sequence and follows the unified power law (Utsu, 1999).

Obtaining the accurate exponent of the power law is a key process in statistical physical analysis. The most widely used method is maximum likelihood estimation, which is not affected by the division of statistical units and can more accurately reflect the characteristics of AE events (Baró and Vives, 2012). Previous studies have shown that the AE energy of the synthetic porous media Vycor glass could span several orders of magnitude and satisfy the power law distribution very well (Salje et al., 2011). For natural rock, the AE energy of natural phosphorus and aluminum minerals shows that the critical exponent of the power law distribution is related to the porosity of porous materials (Nataf et al., 2014b). In addition, many scholars have studied the power law distribution of AEs in the failure processes of rocks with porous brittle characteristics (such as sandstone, shale, and granite) to analyze their failure mechanism (Jiang et al., 2016a; Xie et al., 2018; Salje et al., 2019).

In this study, granite is taken as a common representative

of hot dry rocks and used for mechanical tests to determine the effects of supercritical CO₂ soaking, on failure mechanisms. Additionally, AE-monitoring was performed for all tests to identify diagnostic AE of failure. By means of statistical physical analysis, the distribution characteristics of the maximum likelihood (ML) curve and the change in the critical exponent of AE energy during the failure process of granite are studied. Combined with X-ray diffraction (XRD), scanning electron microscopy (SEM), and optical electron microscopy (Li et al., 2020a), the influence of supercritical CO₂ on the failure mechanism of granite is explored in combination with changes in the mineral composition and microstructure of granite. This study will be of significance for the prediction of artificial earthquakes induced by the development of hot dry rock.

2. Experimental methods

The granite used in the test was from Sichuan Basin, China. All specimens were taken from the same block of rock to reduce effect of specimen differences on the results. The granite was processed into a standard cylindrical specimen of 25 mm × 50 mm, and its surface roughness was within 0.02 mm after polishing (Fig. 1). The average particle diameter was 47.05 μm and the average porosity was 0.83%. A granite soaking experiment was carried out using a self-designed high-temperature and high-pressure CO₂ soaking device (Fig. 2(a)). The device is composed of a sealed tank, a Teledyne ISCO 260D syringe pump (made in USA), and a constant-temperature water bath box. The supercritical CO₂ soaking pressure was set to 13 MPa, the temperature was set to 60 °C, and the soaking time was set to be 24 h (according to the supercritical state of CO₂ and the on-site fracturing time).

Uniaxial compression experiments were carried out on granite specimens before and after supercritical CO₂ soaking. The experimental equipment used was a Shimadzu AGI-250 high-precision material testing machine with a maximum range of 250 kN and a relative accuracy of ± 0.5%. The compression experiment was carried out by displacement loading at a speed of 0.1 mm/min. AE signals were collected using a PCI-2 acoustic emission workstation manufactured by the American Physical Acoustics Company and NANO-30 acoustic emission sensors. This system met the requirements of AE experiments for rock materials. A coupling agent was

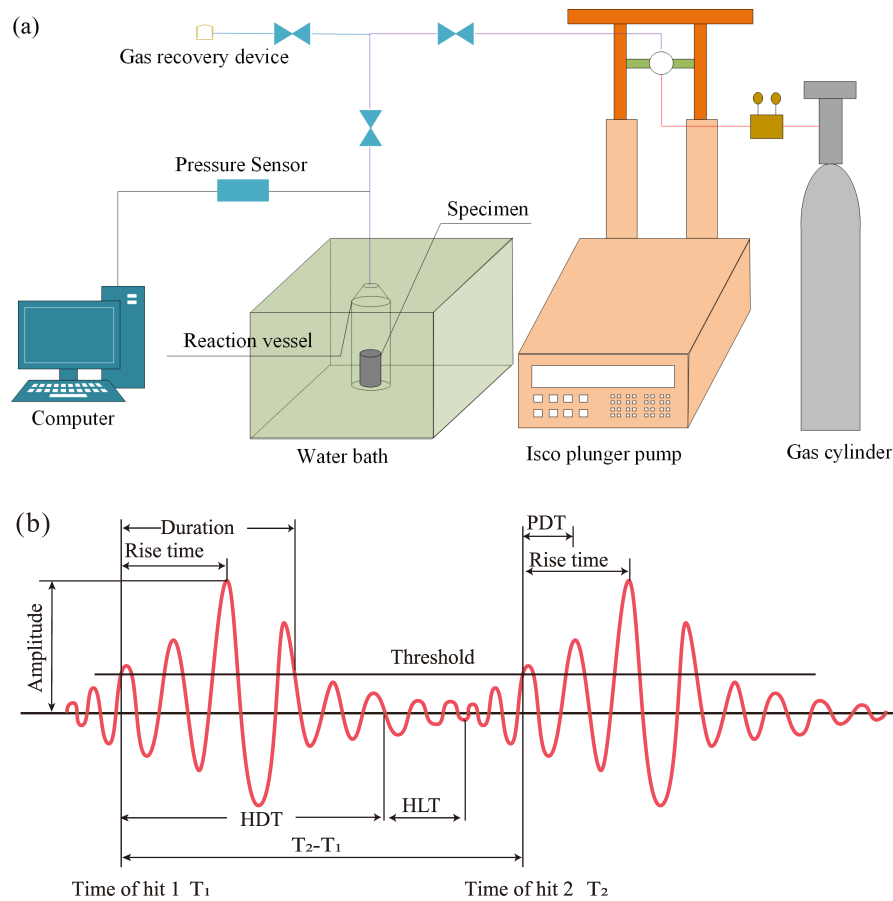


Fig. 2. (a) Schematic diagram of soaking system, (b) supercritical CO₂ soaking device.

applied between the sensors and the specimen surface to ensure good reception of the AE signals. In order to eliminate the influence of background noise on the test, the blank test was used to select the threshold value before the formal test. By continuously lowering the threshold value until the background noise was detected, and on this basis, add 2 dB as the threshold value. For this experiment, the threshold value selected through the blank test was 35 dB, the hit definition time was 150 μ s, the hit locking time was 300 μ s, and the peak definition time was 35 μ s (Fig. 2(b)). To analyze the changes in granite mineral composition before and after supercritical CO₂ soaking, 200 mesh granite powder was prepared and the mineral content was determined by X-ray diffraction. SEM and optical observations were used to observe the effect of supercritical CO₂ soaking on the morphological structure of granite micropores.

3. Experimental results

3.1 Compressive strength and AE energy

The intensity of an AE signal event is directly determined by the amount of energy released inside the rock specimen during deformation and failure (Chang and Lee, 2004; Davidsen et al., 2017). The absolute energy of AE signals is obtained by the fast numerical integration of the square of the acquisition voltage as follows (Nataf et al., 2014a):

$$E = \frac{1}{R} \int_{t_j}^{t_i} U^2(t) dt \quad (1)$$

where E is the absolute energy of the AE signal (aJ) (atto-Joules = 10^{-18} J), t_i and t_j are the starting and ending times of the AE event signals, respectively, and R is the resistance value of the AE acquisition workstation, U is the acquisition signal voltage.

Many studies have shown that the rock strength decreases after the rock is exposed to supercritical CO₂. Two of the most representative specimens have been selected for analysis in this paper. As can be seen from the stress curve in Fig. 3, the compressive strength of granite decreases significantly after it is exposed to supercritical CO₂. With an increase in the load for the untreated granite, there is a long quiet period as AE energy accumulates, and then a sharp increase in AE energy before failure. By contrast, after supercritical CO₂ soaking, energy is actively released by granite, throughout the loading process, and the energy released and stored here is much greater than that in untreated granite. The captured AE signal is the elastic energy released due to the instability of the internal structure of the rock (Li et al., 2020b), therefore the data show that the granite will exhibit more instability related failures in the loading process after supercritical CO₂ soaking.

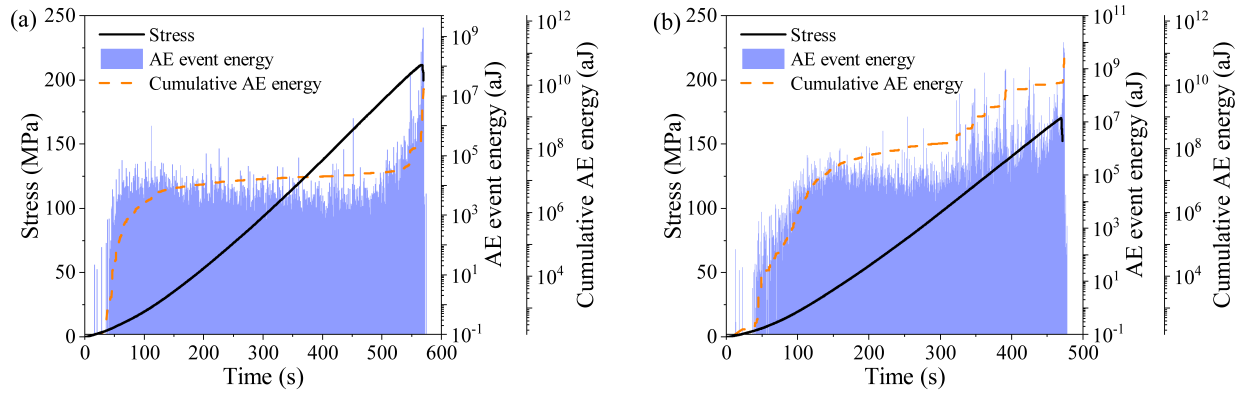


Fig. 3. Stress and AE events energy versus time (a) before and (b) after treatment.

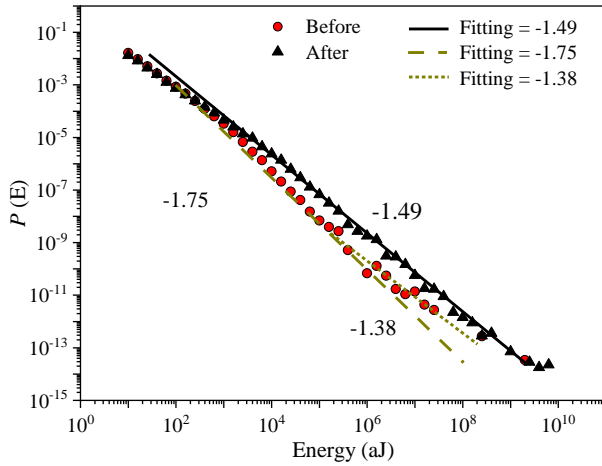


Fig. 4. Log-log plot of the energy distribution of the AE events.

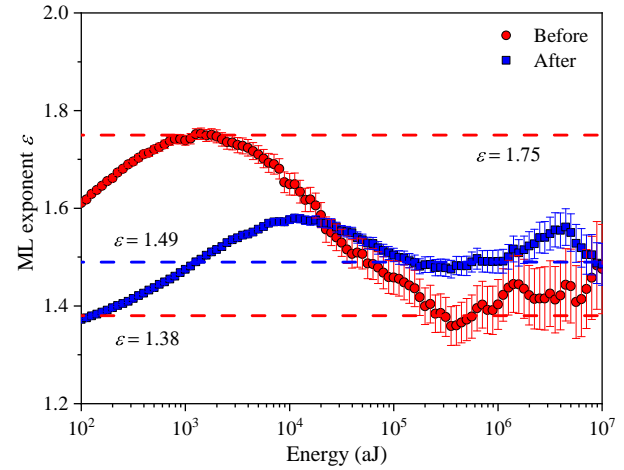


Fig. 5. Lower fitting cut-off as energy exponent.

3.2 Statistical characteristics of AE energy

AE signals are chaotic, therefore, a statistical analysis is necessary to draw a clear comparison of AE signals in different situations. Fig. 4 shows the absolute energy distribution of different samples in logarithmic space. The accumulation of signals during the entire experiment process was expressed by a histogram. The probability distribution function of the absolute energy is $P(E)$. For untreated granite, two types of linear behaviors can be observed by considering two intervals according to 10^4 aJ. The slopes of the two fitting lines are approximately -1.75 and -1.38.

However, for the granite soaked in supercritical CO_2 , a clear linear behavior is observed over more than seven decades in the plot, and the slope of the fitting line is -1.49. This indicates that the distribution of AE energy in granite follows the power law, which can be described as follows (Clauset et al., 2009; Castillo-Villa et al., 2013):

$$P(E)dE = \frac{E^{-\varepsilon}}{E_{\min}^{1-\varepsilon}} dE \quad E > E_{\min} \quad (2)$$

where E_{\min} is a lower cutoff, and ε is the exponent, usually between 1 and 2.5 (Salje and Dahmen, 2014).

In order to avoid errors caused by the construction of the histogram (direct binning method), the maximum likelihood

method was used to obtain more reliable power law exponents (Goldstein et al., 2004; Bauke, 2007; Castillo-Villa et al., 2013). The formula is as follows:

$$\varepsilon(x_{\min}) = 1 + n \left(\sum_{i=1}^n \ln \frac{x_i}{x_{\min}} \right)^{-1} \quad (3)$$

where x_i , $i = 1, \dots, n$ are the observation values satisfying $x_i \geq x_{\min}$.

The standard error is:

$$\delta = \frac{\varepsilon(x_{\min}) - 1}{\sqrt{n}} + O\left(\frac{1}{n}\right) \quad (4)$$

where δ is the standard error, O means infinitesimal of higher order.

The exponent ε can be estimated through the platform section of the curve. Fig. 5 shows the analysis results, which are consistent with the results of the direct binning method shown in Fig. 4. The horizontal dotted lines in the figure comes from the slopes of the distribution line of the histogram. For the AE energy distribution with a small exponent, the slope is gentle, which indicates that the AE signals are dominated by large AE energy events. Previous studies have shown that the power law index of AE energy can reflect the inner structure and degree of damage in porous materials (Pan et al., 2018). Higher exponent values usually occur under conditions of

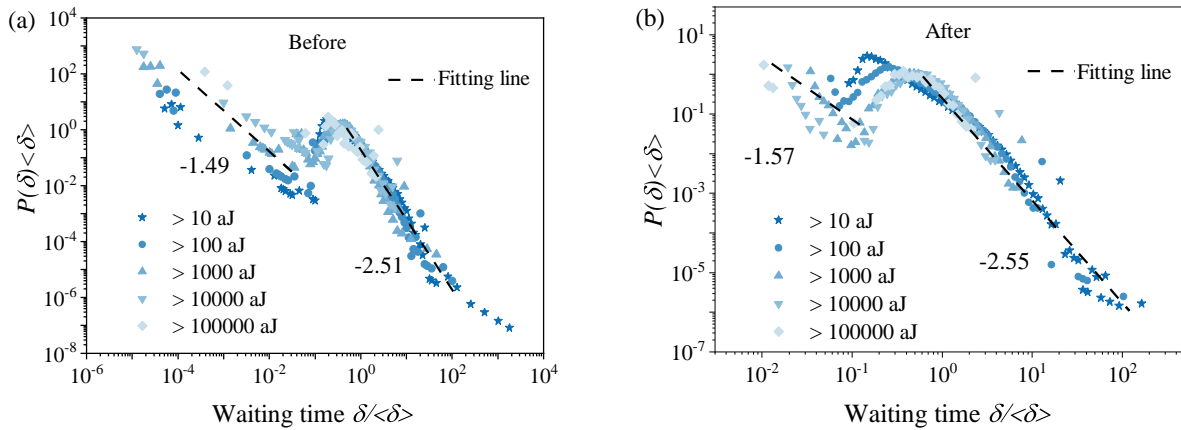


Fig. 6. Distribution of waiting time after renormalization (a) before and (b) after treatment.

friction, and lower values are a result of fractures (Soto-Parra et al., 2018). In addition, the mean field theory predicts that the distribution exponent of the fracture mechanism is $1/3$ (Salje and Dahmen, 2014). For the untreated granite, there was a decrease in the AE energy distribution exponent. This decrease is the result of the combined effect of the fracture and friction mechanisms (Jiang et al., 2016b). This decrease is consistent with many intact rock compression results (Jiang et al., 2017). However, the granite after supercritical CO_2 soaking did not show an obvious exponent decrease, indicating that this combined effect was weak.

In addition to the AE energy distribution described above, the temporal distribution is also an important aspect of avalanche dynamic characteristics. These temporal distributions can be described by the waiting time. Waiting time refers to the time interval between two adjacent AE pulses (Kun et al., 2013; Xie et al., 2019), which is defined as $\delta_j = t_j - t_{j-1}$, where the energy of the j event must be larger than the threshold energy E_{\min} . According to the universal scaling law (Baró et al., 2013; Nataf et al., 2014a), after normalization by its average, the distribution of waiting time collapses into a single or double power law. As shown in Fig. 6, the statistical distribution characteristics remain unchanged with an increase in the energy threshold ($E > 10^0$ aJ, 10^1 aJ, 10^2 aJ). According to the literature (Corral, 2003), for systems with non-stationary activity rates, the AE statistical distribution of granite conforms to the seismic statistical distribution law both before and after supercritical CO_2 soaking and can be determined using the double power law curve. For small arguments, the exponents are approximately 1.5. In case of large arguments, the exponents are approximately 2.5; these values are similar to those reported by Jiang et al. (2016b) and to some SiO_2 -based materials (Nataf et al., 2014a).

4. Discussion

4.1 Super-jerk rank analysis

The failure of rock does not occur at a single fixed critical point but may be a result of the combination of the power law at different stages. To further understand the critical

characteristics during the failure process of granite before and after supercritical CO_2 soaking, AE events in the failure process were divided into intervals by the super-jerk method (Jiang et al., 2017). As avalanche signals, if the energy of AE signals is greater than that of any event in a previous series, it is defined as a super-jerk and numbered by the rank $k = 1, 2, \dots, n$. The complete AE series is divided into many small subsets. Fig. 7 shows the results of the super-jerk analysis before and after supercritical CO_2 soaking. Fig. 8 shows the maximum likelihood estimation for different super-jerk intervals. It also requires a certain number of samples in the superjerks energy interval to ensure the accuracy of the maximum likelihood estimation results. Superjerks appeared very quickly in the early stage, resulting in a small number of events in the superjerks intervals. Therefore, we combined multiple superjerks intervals in the early stage for maximum likelihood estimation analysis. For untreated granite, the critical exponents decreased approximately from 1.7 to 1.4 over time. Corresponding to the total exponential change, the mixing of exponentials reflects the superposition and interaction of the rock fracture mechanism (critical exponents); that is, the failure mechanism of untreated granite is a combination of the two failure mechanisms. However, for the granite after supercritical CO_2 soaking, the exponents of the subset have little correlation with time, and most of them are approximately 1.6.

The global maximum likelihood estimate results are the superposition of the results for each super-jerk interval (Fig. 8). Comparing the two cases, both untreated granite and treated granite have a low exponent stage of less than 1.3. However, for untreated granite, the low exponent phenomenon is more obvious, which is also the reason for the decline in the overall maximum likelihood curve. The theoretical value of the fracture mechanism is 1.3 (Jiang et al., 2017). It was observed that the integrity of the untreated granite sample was better, and the energy released from fracture brittleness played a dominant role. For the granite after supercritical CO_2 soaking, the friction between mineral particles could not be ignored due to internal damage. The energy distribution no

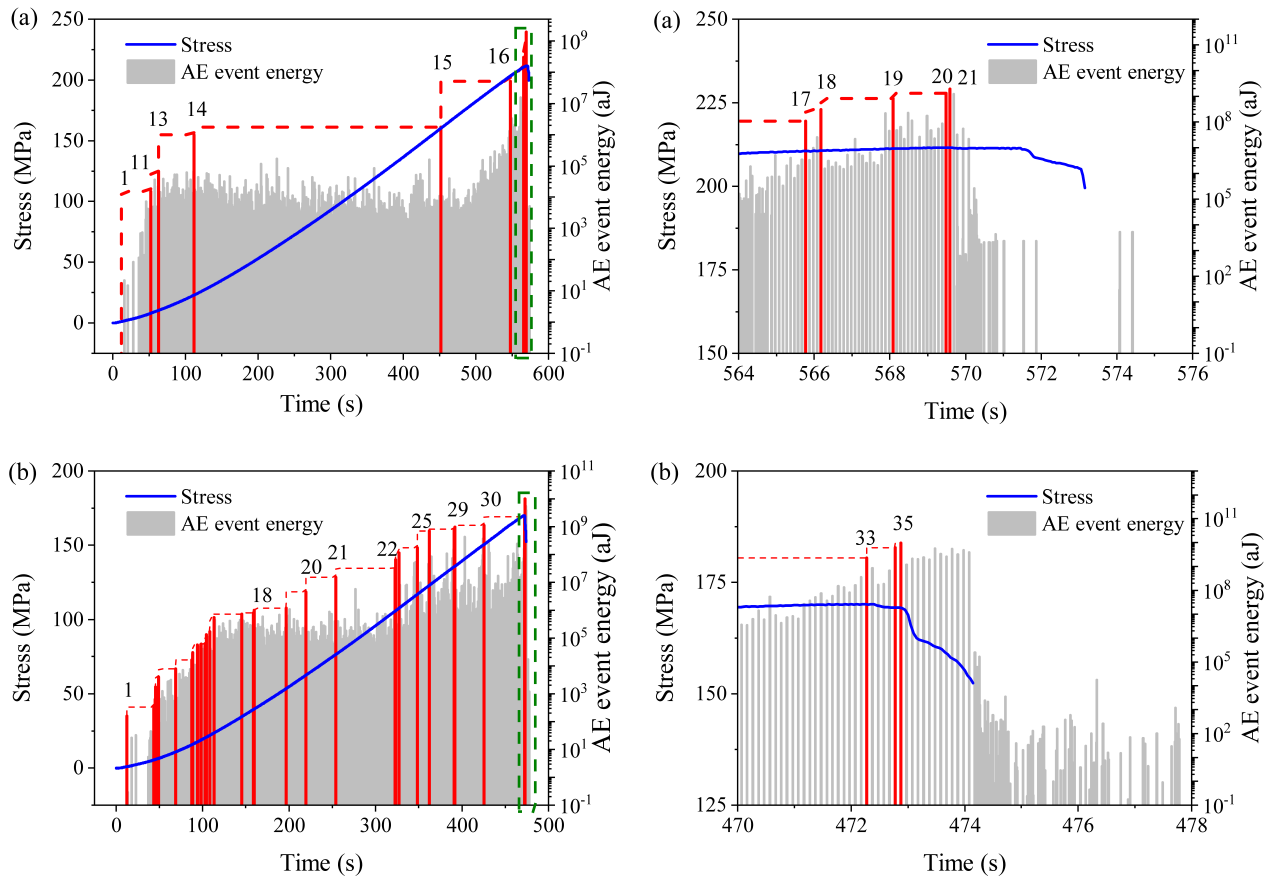


Fig. 7. Time sequence of jerk events in granite under uniaxial stress (a) before and (b) after treatment.

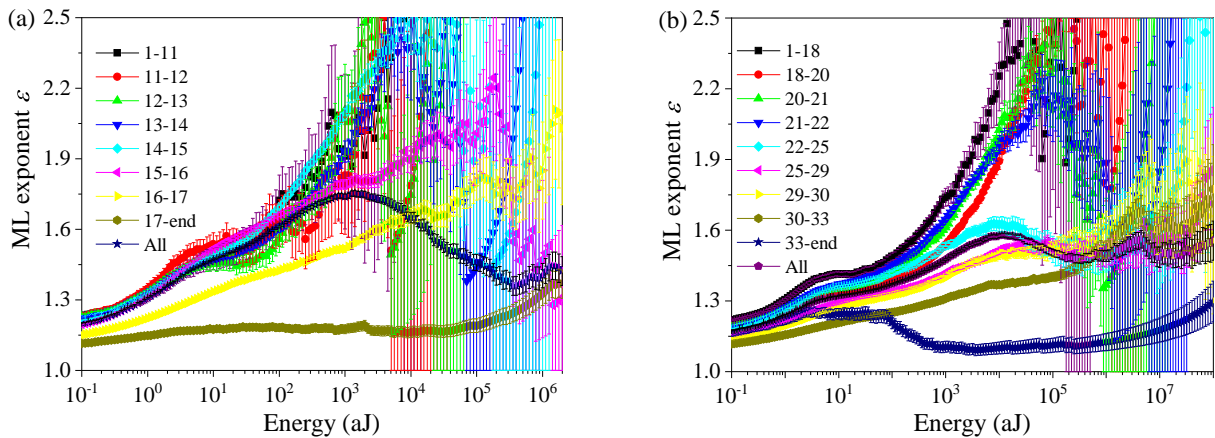


Fig. 8. ML curves with energy exponent for different super-jerk ranks (a) before and (b) after treatment.

longer satisfied the pure power law but was the product of the power law and an exponential damping factor, which can be further investigated using the maximum likelihood curve as explained in the next section.

4.2 Mixing and damping analysis

The theoretical distribution models of the maximum likelihood critical exponent mainly fall into three categories (Salje and Dahmen, 2014; Salje et al., 2019). The first is the pure

power law, where the exponent value is constant among several orders of magnitude. The second is power mixing, where the exponential curve varies between different orders of magnitude, and as the mixing is affected by two pure power laws of different mechanisms, the curve exhibits an inverted “S” shape, which can be described by the maximum likelihood exponent method based on double power laws. The third is exponential damping, where the maximum likelihood curve continues to rise. The maximum likelihood curve of AE energy

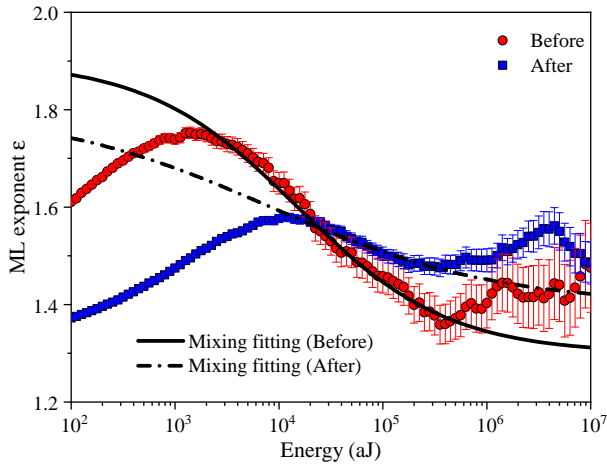


Fig. 9. Exponential mixing theory used to fit the maximum likelihood curve.

that satisfies the single power law can be fitted by the probability density function model considering the damping effect. The above analysis shows that the AE energy of the entire failure process of both untreated and treated granite satisfies the characteristics of power laws mixing, and the rock sample before supercritical CO₂ soaking shows more obvious mixing effect. The continuous increasing maximum likelihood curves before collapse obey the product of the power law and an exponent, which is introduced by the damping effect of friction. The formula for the maximum likelihood exponent method based on the double power law in the literature (Eq. (5)) is used to fit the experimental data (Xie et al., 2019). For untreated granite, the fixed critical points of the two pure power laws are 1.9 (upper limit) and 1.3 (lower limit) ($\beta = 91\%$). For treated granite, the fixed critical points of the two pure power laws are 1.8 (upper limit) and 1.4 (lower limit) ($\beta = 78\%$). The theoretical fitting curve is consistent with the experimental data, which verifies the accuracy of the mixing effect of the pure power laws (Fig. 9).

$$\gamma = 1 + \frac{\alpha \left(\frac{E_{\min}}{E_0}\right)^{\alpha-1} + (1-\alpha) \left(\frac{E_{\min}}{E_0}\right)^{\beta-1}}{\frac{\alpha}{\alpha-1} \left(\frac{E_{\min}}{E_0}\right)^{\alpha-1} + \frac{1-\alpha}{\beta-1} \left(\frac{E_{\min}}{E_0}\right)^{\beta-1}} \quad (5)$$

where γ is the fitting index, E_0 is the cutoff values, and α and β are the upper and lower power values, respectively.

The probability density function model (Eq. (6)) considering the damping effect can be used to fit the experimental data of treated granite (Salje et al., 2017). When $\alpha = 1.25$, $\Lambda = 80,000$, the maximum likelihood curve calculated by the model can well reflect the variation characteristics of the real power values (Fig. 10).

$$g(E)dE = \frac{E^{-\alpha} \exp\left(-\frac{E}{\Lambda}\right) dE}{\int_{E_{\min}}^{\infty} E^{-\alpha} \exp\left(-\frac{E}{\Lambda}\right) dE} \quad E > E_{\min} \quad (6)$$

where Λ is the damping coefficient of energy.

Damping in this paper mainly means that the damping term of exponential function is added to the maximum likelihood estimation, which is a mathematical expression. In physical systems, this damping effect can come from many factors, su-

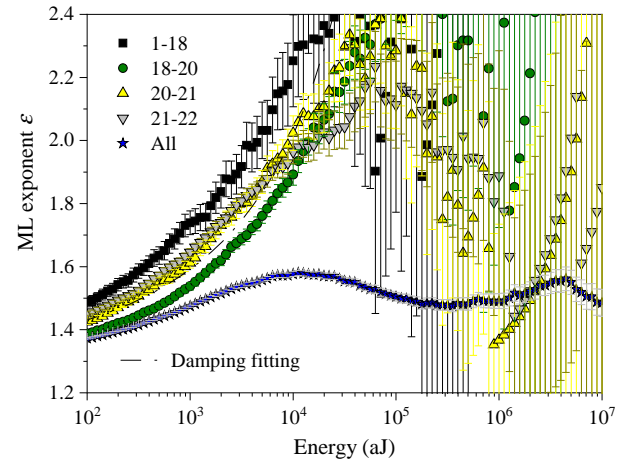


Fig. 10. Exponential damping theory used to fit the maximum likelihood curve for granite soaked in supercritical CO₂.

ch as the limitations of test equipment and other energy dissipation mechanisms such as friction.

By comparing the results of the two types of granite samples discussed above, it can be seen that the stage near the failure point has a considerable influence on the entire compression process. Upon observing the temporal distribution of waiting time for untreated granite, there were many AE events with a waiting time < 0.0001 s (the circle in Fig. 11(a)) near failure, corresponding to the 17-end stage in the super-jerk analysis (Figs. 7(a) and 8(a)). This stage depicts an obvious mixing effect of two failure mechanisms in the maximum likelihood curve. For the treated granite, there was no AE event with a waiting time < 0.0001 s when approaching failure, the maximum likelihood curve did not decrease substantially, and the mixing effect of the two failure mechanisms was not obvious. This result is consistent with the waiting time distribution in Fig. 4.

4.3 XRD and SEM

When shale, granite and other rocks are exposed to supercritical CO₂, the water molecules in rock minerals combine with the CO₂ to form carbonic acid and dissolve calcite, feldspar and other mineral particles (Cai et al., 2018; Zhou et al., 2019; Li et al., 2020a). It can be seen from Table 1 that the granite mineral composition changes significantly after supercritical CO₂ soaking, with a significant decrease in the calcite content. The phenomenon of mineral dissolution can also be observed from the optical observations (Fig. 12) and SEM images (Fig. 13). In addition, the granite after supercritical CO₂ soaking has more cracks and pores as compared to the untreated granite. The microstructure of rocks is an important factor affecting their macroscopic mechanical properties (Lu et al., 2019); therefore, it is considered that a change in the fracture mechanism (critical exponent) in the failure process of granite soaked by supercritical CO₂ is mainly caused by a change in its microscopic pore structure. The untreated granite is intact and dense, and the fracture mechanism is the dominant factor during the failure process; therefore, the maximum likelihood curve could be lowered due to the fracture mechanism. The internal damage of the granite

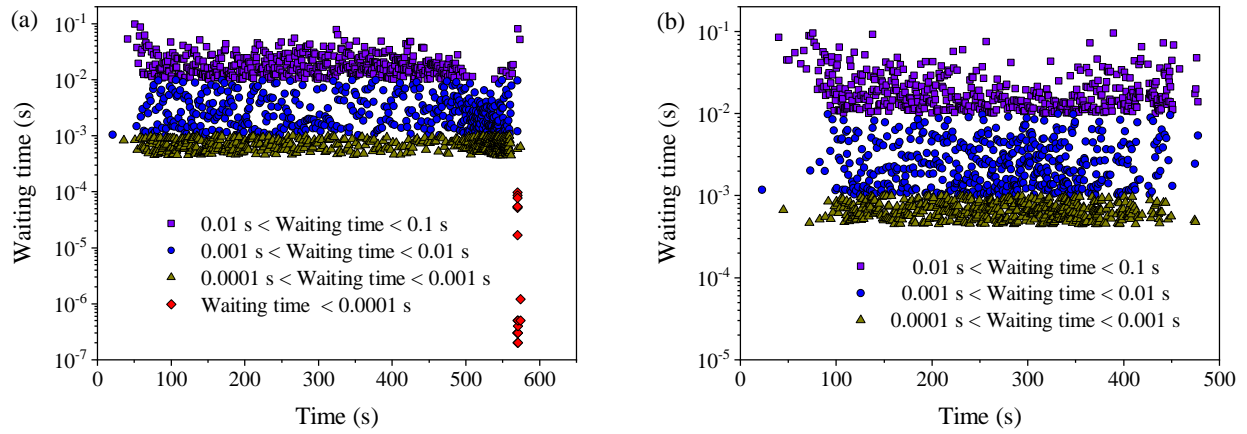


Fig. 11. Waiting time versus time (a) before and (b) after treatment.

Table 1. Mineral analysis of granite (%).

Mineral	Quartz	Plagioclase	Potash feldspar	Anhydrite	Gibbsite	Calcite	Dolomite	Siderite	Magnesite
Before	37.7	23.8	25.5	4.3	2.7	2.2	2	0.8	1
After	32.6	31.7	25.1	4.1	2.8	0.8	1	0.7	1.2

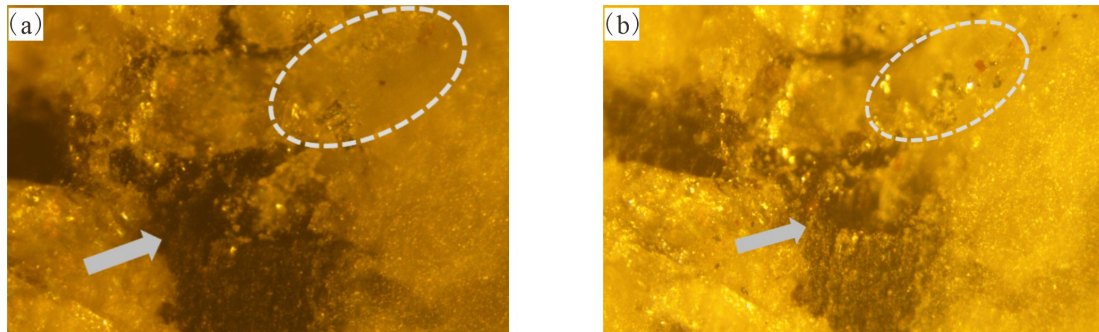


Fig. 12. Microscopic observations of granite (a) before and (b) after treatment.

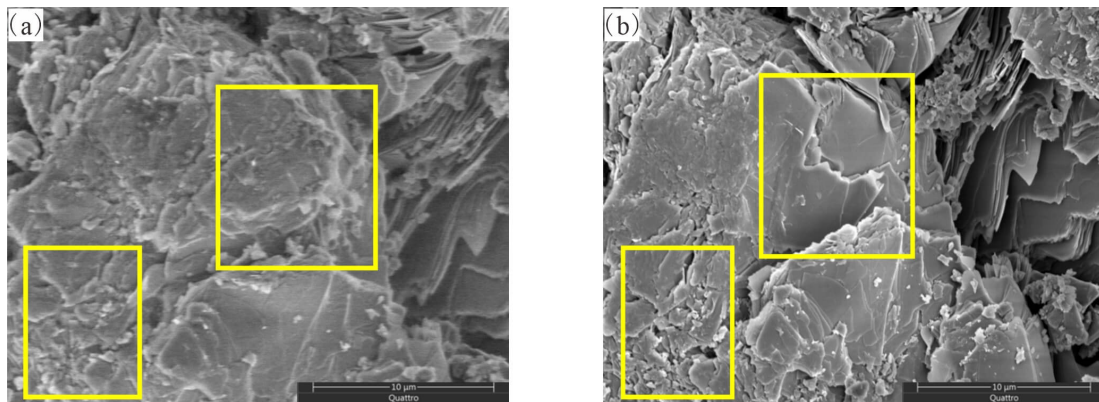


Fig. 13. SEM images of granite (a) before and (b) after treatment.

treated with supercritical CO₂ resulted in the crumbing of the granite. The friction mechanism during failure could not be ignored and the shape of the exponential curve exhibited a damping effect.

5. Conclusions

Uniaxial compression tests of granite before and after supercritical CO₂ soaking were carried out, and the AE energy of the entire failure process was simultaneously investigated. The following conclusions were drawn:

The compressive strength of granite decreased after supercritical CO₂ soaking. Before the failure of untreated granite, the AE events exhibited a long quiet period, and the power law exponent showed an obvious decrease. By contrast, for the granite treated with supercritical CO₂, AE events were very active throughout the loading process, and the power law exponent of energy decreased only slightly.

The global maximum likelihood curve is the superposition of the ML curves for each super-jerk interval. The untreated granite was completely intact; there were several AE events with a waiting time < 0.0001 s when approaching failure. The failure mechanism exhibited a typical combined effect of the fracture and friction mechanisms, and the maximum likelihood curve could be fitted by mixing double power laws of 1.8 and 1.4. Affected by the dissolution of minerals such as calcite, the microstructure of granite changed after supercritical CO₂ soaking, resulting in new cracks and pores. Furthermore, the observation of crumbing in the soaked granite shows that friction-dependent mechanisms are important for the entire failure process in granite, and should not be ignored. The maximum likelihood curve showed a damping effect, which followed the product of the power law and an exponential damping factor. In general, the AE statistical distribution of granite conformed to the seismic statistical distribution law before and after supercritical CO₂ soaking. This study is conducive to the further understanding of artificial earthquakes induced by the development of hot dry rock.

Acknowledgement

The authors are grateful to the National Natural Science Foundation of China (Nos. 51904042, 52178313 and 51908088). The authors also thank the Natural Science Foundation of Chongqing (No. cstc2019jcyj-xfxkX0001).

Conflict of interest

The authors declare no competing interest.

Open Access This article is distributed under the terms and conditions of the Creative Commons Attribution (CC BY-NC-ND) license, which permits unrestricted use, distribution, and reproduction in any medium, provided the original work is properly cited.

References

- Anyim, K., Gan, Q. Fault zone exploitation in geothermal reservoirs: Production optimization, permeability evolution and induced seismicity. *Advances in Geo-Energy Research*, 2020, 4(1): 1-12.
- Baisch, S., Weidler, R., Vörös, R., et al. A conceptual model for post-injection seismicity at Soultz-sous-Forêts. *Transactions-Geothermal Resources Council*, 2006, 30: 601-605.
- Baró, J., Corral, A., Illa, X., et al. Statistical similarity between the compression of a porous material and earthquakes. *Physical Review Letters*, 2013, 110(8): 088702.
- Baró, J., Vives, E. Analysis of power-law exponents by maximum-likelihood maps. *Physical Review E*, 2012, 85(6): 066121.
- Bauke, H. Parameter estimation for power-law distributions by maximum likelihood methods. *The European Physical Journal B*, 2007, 58: 167-173.
- Beckers, K. F., Lukawski, M. Z., Anderson, B. J., et al. Levelized costs of electricity and direct-use heat from Enhanced Geothermal Systems. *Journal of Renewable and Sustainable Energy*, 2014, 6(1): 013141.
- Bongole, K., Sun, Z., Yao, J., et al. Multifracture response to supercritical CO₂-EGS and water-EGS based on thermo-hydro-mechanical coupling method. *International Journal of Energy Research*, 2019, 43(13): 7173-7196.
- British Columbia Oil and Gas Commission. Investigation of observed seismicity in the Horn River basin. Technical Report, 2012.
- Cai, C., Kang, Y., Wang, X., et al. Mechanism of supercritical carbon dioxide (SC-CO₂) hydro-jet fracturing. *Journal of CO₂ Utilization*, 2018, 26: 575-587.
- Castillo-Villa, P. O., Baró, J., Planes, A., et al. Crackling noise during failure of alumina under compression: The effect of porosity. *Journal of Physics: Condensed Matter*, 2013, 25(29): 292202.
- Chang, S. H., Lee, C. I. Estimation of cracking and damage mechanisms in rock under triaxial compression by moment tensor analysis of acoustic emission. *International Journal of Rock Mechanics and Mining Sciences*, 2004, 41(7): 1069-1086.
- Clauset, A., Shalizi, C. R., Newman, M. E. J. Power-law distributions in empirical data. *SIAM Review*, 2009, 51(4): 661-703.
- Corral, A. Local distributions and rate fluctuations in a unified scaling law for earthquakes. *Physical Review E*, 2003, 68(3): 035102R.
- Davidson, J., Kwiatek, G., Charalampidou, E. M., et al. Triggering processes in rock fracture. *Physical Review Letters*, 2017, 119(6): 068501.
- Duchane, D., Brown, D. Hot dry rock (HDR) geothermal energy research and development at Fenton Hill, New Mexico. *Geo-Heat Centre Quarterly Bulletin*, 2002, 23: 13-19.
- Eberhardt, E., Stead, D., Stimpson, B. Quantifying progressive pre-peak brittle fracture damage in rock during uniaxial compression. *International Journal of Rock Mechanics and Mining Sciences*, 1999, 36(3): 361-380.
- Ershadnia, R., Wallace, C. D., Soltanian, M. R. CO₂ geological sequestration in heterogeneous binary media: Effects of geological and operational conditions. *Advances in Geo-Energy Research*, 2020, 4(4): 392-405.
- Garcia, J., Hartline, C., Walters, M., et al. The northwest geysers EGS demonstration project, California: Part 1: Characterization and reservoir response to injection. *Geothermics*, 2016, 63: 97-119.
- Goldstein, M. L., Morris, S. A., Yen, G. G. Problems with fitting to the power-law distribution. *The European Physical Journal B-Condensed Matter and Complex Systems*, 2004, 41(2): 255-258.
- Haering, M. O., Schanz, U., Ladner, F., et al. Characterisation of the Basel 1 enhanced geothermal system. *Geothermics*, 2008, 37(5): 469-495.
- Hofmann, H., Weides, S., Babadagli, T., et al. Potential

- for enhanced geothermal systems in Alberta, Canada. *Energy*, 2014, 69: 578-591.
- Hou, Z. M., Kracke, T., Zhou, L., et al. Rock mechanical influences of hydraulic fracturing deep underground the North German Basin: Geological integrity of the cap rock salt and maximum magnitude of induced microseismicity based on the GeneSys stimulation in May 2011. *Erdöl Erdgas Kohle*, 2012, 11: 454-460.
- Jiang, X., Jiang, D., Chen, J., et al. Collapsing minerals: Crackling noise of sandstone and coal, and the predictability of mining accidents. *American Mineralogist*, 2016b, 101(12): 2751-2758.
- Jiang, X., Liu, H., Main, I. G., et al. Predicting mining collapse: Superjerks and the appearance of record-breaking events in coal as collapse precursors. *Physical Review E*, 2017, 96(2): 023004.
- Jiang, D., Xie, K., Jiang, X., et al. Statistical analysis of acoustic emission energy distribution during uniaxial compression of shale. *Chinese Journal of Rock Mechanics and Engineering*, 2016a, 35(S2): 3822-3828. (in Chinese)
- Kim, J. S., Lee, K. S., Cho, W. J., et al. A comparative evaluation of stress-strain and acoustic emission methods for quantitative damage assessments of brittle rock. *Rock Mechanics and Rock Engineering*, 2015, 48: 495-508.
- Kim, K. H., Ree, J. H., Kim, Y., et al. Assessing whether the 2017 M_w 5.4 Pohang earthquake in South Korea was an induced event. *Science*, 2018, 360(6392): 1007-1009.
- Kun, F., Varga, I., Lennartz-Sassinek, S., et al. Approach to failure in porous granular materials under compression. *Physical Review E*, 2013, 88(6): 062207.
- Legarth, B., Huenges, E., Zimmermann, G. Hydraulic fracturing in a sedimentary geothermal reservoir: Results and implications. *International Journal of Rock Mechanics and Mining Sciences*, 2005, 42(7-8): 1028-1041.
- Li, H., Zhou, L., Lu, Y., et al. Changes in pore structure of dry-hot rock with supercritical CO₂ treatment. *Energy & Fuels*, 2020a, 34(5): 6059-6068.
- Li, H., Zhou, L., Lu, Y., et al. Influence of supercritical CO₂ saturation on the failure process of hot dry rock with acoustic emission monitoring. *Powder Technology*, 2020b, 374: 241-249.
- Lu, Y., Chen, X., Tang, J., et al. Relationship between pore structure and mechanical properties of shale on supercritical carbon dioxide saturation. *Energy*, 2019, 172: 270-285.
- Luo, F., Xu, R., Jiang, P. Numerical investigation of fluid flow and heat transfer in a doublet enhanced geothermal system with CO₂ as the working fluid (CO₂-EGS). *Energy*, 2014, 64: 307-322.
- Nataf, G. F., Castillo-Villa, P. O., Baró, J., et al. Avalanches in compressed porous SiO₂-based materials. *Physical Review E*, 2014a, 90(2): 022405.
- Nataf, G. F., Castillo-Villa, P. O., Sellappan, P., et al. Predicting failure: Acoustic emission of berlinite under compression. *Journal of Physics: Condensed Matter*, 2014b, 26(27): 275401.
- Pan, X., Chen, J., Jiang, D., et al. Statistical characteristics of sandstone acoustic emission under triaxial unloading confining pressure. *Journal of China Coal Society*, 2018, 43(10): 2750-2757. (in Chinese)
- Salje, E. K. H., Dahmen, K. A. Crackling noise in disordered materials. *Annual Review of Condensed Matter Physics*, 2014, 5(1): 233-254.
- Salje, E. K. H., Liu, H., Xiao, Y., et al. Avalanche mixing and the simultaneous collapse of two media under uniaxial stress. *Physical Review E*, 2019, 99(2): 023002.
- Salje, E. K. H., Planes, A., Vives, E. Analysis of crackling noise using the maximum-likelihood method: Power-law mixing and exponential damping. *Physical Review E*, 2017, 96(4): 042122.
- Salje, E. K. H., Soto-Parra, D. E., Planes, A., et al. Failure mechanism in porous materials under compression: Crackling noise in mesoporous SiO₂. *Philosophical Magazine Letters*, 2011, 91(8): 554-560.
- Sathar, S., Worden, R. H., Faulkner, D. R., et al. The effect of oil saturation on the mechanism of compaction in granular materials: Higher oil saturations lead to more grain fracturing and less pressure solution. *Journal of Sedimentary Research*, 2012, 82(8): 571-584.
- Soto-Parra, D., Vives, E., Botello-Zubiate, M. E., et al. Acoustic emission avalanches during compression of granular manganites. *Applied Physics Letters*, 2018, 112(25): 251906.
- Utsu, T. Representation and analysis of the earthquake size distribution: A historical review and some new approaches. *Pure and Applied Geophysics*, 1999, 155: 509-535.
- Xie, K., Jiang, X., Jiang, D., et al. Change of crackling noise in granite by thermal damage: Monitoring nuclear waste deposits. *American Mineralogist*, 2019, 104(11): 1578-1584.
- Xie, K., Jiang, D., Sun, Z., et al. NMR, MRI and AE statistical study of damage due to a low number of wetting-drying cycles in sandstone from the Three Gorges Reservoir Area. *Rock Mechanics and Rock Engineering*, 2018, 51: 3625-3634.
- Xu, T., Zhang, Y., Zeng, Z., et al. Technology progress in an enhanced geothermal system (hot dry rock). *Science & Technology Review*, 2012, 30(32): 42-45. (in Chinese)
- Yin, H., Zhou, J., Xian, X., et al. Experimental study of the effects of sub- and super-critical CO₂ saturation on the mechanical characteristics of organic-rich shales. *Energy*, 2017, 132: 84-95.
- Zhang, C., Liang, W., Li, Z., et al. Observations of acoustic emission of three salt rocks under uniaxial compression. *International Journal of Rock Mechanics and Mining Sciences*, 2015, 77: 19-26.
- Zhou, J., Hu, N., Xian, X., et al. Supercritical CO₂ fracking for enhanced shale gas recovery and CO₂ sequestration: Results, status and future challenges. *Advances in Geo-Energy Research*, 2019, 3(2): 207-224.